Korean J. Chem. Eng., 34(10), 2756-2763 (2017)
DOI: 10.1007/s11814-017-0168-0

pISSN: 0256-1115
eISSN: 1975-7220

Gasification characteristics of glass fiber-reinforced plastic (GFRP) wastes in a microwave plasma reactor

Young Min Yun*, Myung Won Seo,†, Ho Won Ra**, Sang Jun Yoon**, Tae-Young Mun**, Ji-Hong Moon**, Jin Woo Kook**, Yong Ku Kim**, Jae Goo Lee**, and Jae Ho Kim**,†**

*Plasma Team, Vitzro Tech, Ansan, Gyonggi-do 15603, Korea
**Clean Fuel Laboratory, Korea Institute of Energy Research (KIER), Daejeon 34129, Korea
(*Received 8 February 2017 • accepted 20 June 2017*)

Abstract−The effects of plasma power (1-1.8 kW), oxygen/fuel (0-2.5) and steam/fuel ratios (0-1) on the gasification characteristics of glass fiber-reinforced plastic (GFRP) wastes have been determined in a microwave plasma reactor. GFRP, which is thermosetting plastic composed of glass fibers embedded within a polymer matrix, was used as an experimental sample. While carbon conversion increased with oxygen/fuel ratio, syngas heating value and cold gas efficiency decreased with oxygen supply due to the onset of combustion. With increasing steam/fuel ratio, water-gas shift and ion-reforming reaction favored higher concentration of H_2. Increasing the plasma power was found to promote the conversion of carbon dioxide to carbon monoxide. The char surfaces of GFRP that were subjected to variable power and oxygen supplies were analyzed by scanning electron microscopy.

Keywords: Microwave Plasma, Glass Fiber-reinforced Plastic, Gasification, Scanning Electron Microscopy

INTRODUCTION

Because of their excellent thermal insulation, impact resistance, and sound absorption characteristics, glass fiber-reinforced plastics (GFRPs) are representative thermosetting plastics employed within building interiors and commonly used by the shipping, automotive, and aerospace industries [1]. The market demand for GFRP continues to increase due to its wide range of applicability and low cost. However, proper treatments and recycling methods have not been developed for use within domestic and industrial markets because of the insolubility and infusibility of these highly networked polymers.

Alternative waste processing methods are necessary to alleviate the environmental impact caused by conventional disposal processing, including landfill dumping and incineration, both of which release harmful gaseous contaminants. Unlike previously employed treatment technologies, waste gasification/pyrolysis produces synthesis gas (syngas), primarily containing hydrogen and carbon monoxide. Applications for syngas are usually classified as follows: (1) steam production, (2) syngas turbines and engines, (3) fuel cells, (4) pure hydrogen production, and (5) various chemical component sources.

Whereas low-grade fuel gasifiers use an autothermal reforming reaction to maintain process temperatures, plasma reactors employ external sources of electricity to achieve much higher temperatures than can be obtained using conventional technologies [2]. Plasma gasification takes advantage of ions, radicals, and electrons that rapidly not only decomposed toxic materials but also convert waste to syngas. This technology is applicable to waste containing a wide range of particle sizes, chemical characteristics, and moisture contents. By introducing steam into a plasma reactor, pure hydrogen can be produced, with the minimal formation of carbon dioxide. This method not only avoids the production of atmospheric pollutants such as NO_x (nitrogen oxides), SO_x (sulfur oxides), and volatile organic compounds (VOCs), but also exhibits better overall reactivity and efficiency [3,4]. After the plasma gasification reaction is completed, the remaining slag, composed of inorganic substances, can be used as a construction material [5,6].

An experiment was carried out using a microwave plasma torch which has longer operation time than a DC-arc-torch. Arc electrodes have a limited life expectancy since they are vulnerable to oxidation, whereas the microwave plasma could not be sustained by using an electrode generator. A resonant cavity for maintaining the plasma is not required, and the microwave plasma efficiency is typically close to 100% in this device. This system also has a simpler structure and is more economical than other plasma generators [7]. The electrokinetic energy of microwave generated plasma (5-15 eV) was found to be greater than that produced by a low-RF discharge. Also the operating pressure range is wider than that of other plasma generators [8].

Studies on gasification of coal and waste in various plasma reactors are summarized in Table 1 [9-12].

All of the experiments were performed on a lab-scale unit. Hong et al. and Yoon et al. [9,10] attempted to generate a syngas from the various coals using the microwave plasma gasifier. Shie et al. [11] carried out batch and continuous plasma reactors and presented optimum time condition in the reactor. Although Tang and Huang carried out biomass plasma pyrolysis in a coupled RF (Radio Frequency) reactor, the experimental device was operated in a low pressure condition [12]. It was reported that a few researchers carried out a

†To whom correspondence should be addressed.
E-mail: jaeho@kier.re.kr, mwseo82@kier.re.kr
‡5th International Conference on Gasification and Its Application.

Table 1. Previous study on plasma gasification

Authors	Plasma type	Sample	Forming gas	Power [kW]	Syngas composition [%]			
					H_2	CO	CH_4	CO_2
Hong et al. [9]	Microwave plasma	Brown coal	Steam	4	35-50	13-25	5	25-45
Yoon et al. [10]	Microwave plasma	Shenhua, WIRA coal	Air, steam	5	20-60	15-45	1-5	17-32
Shie et al. [11]	Arc	Lignocellulosic waste	Nitrogen	10	36-53	36-53	2-5	5-8
Tang and Hong [12]	Radio frequency	Wood	Nitrogen	1.6-2	15-30	19-39	4-13	4-8

GFRP gasification experiment using plasma reactors.

In this study, the gasification characteristics of GFRP in 2 kW microwave plasma reactor were investigated under a range of operating conditions. Within this system, the gasification operating values of plasma power (1-1.6 kW), steam/fuel ratio (0-1), and oxygen/fuel ratio (0-2.5) on the thermal decomposition and gasification characteristics were determined. The GFRP surface, char from pyrolysis, partial oxidation, and steam gasification, were observed by SEM (Scanning Electron Microscopy).

EXPERIMENTAL

1. Materials

GFRP is the byproduct from a ship and chemical solution storage tank manufacturing process. We collected samples by using a standard method (ASTM D6051-96). It was crushed, and pulverized to less than 300 μm to avoid heat and mass transfer limitation. The proximate analysis (ASTM D5142), ultimate analysis (ASTM D3176), and ash-component analysis along with corresponding caloric values (ASTM D3523) of GFRP are presented in Table 2.

GFRP heating value is higher than biomass and therefore more amenable to fuel-reforming technologies. The ultimate analysis showed that the hydrogen was also higher than the coal content [9,10], suggesting that a greater amount of hydrogen concentration, which was evolved from GFRP gasification, should be higher than coal gasification processing. Because the glass fiber is added to enhance the heat and resistance, the important component of the GFRP ash is silica (SiO_2).

Table 2. Proximate, ultimate, calorific value, and ash composition analysis of the GFRP sample

Proximate analysis (wt%, as received)		Ultimate analysis (wt%, daf)	
Moisture	1.57	C	77.814
Volatile matter	71.19	H	6.934
Fixed carbon	5.04	N	0.568
Ash	22.2	O[a]	14.683
Higher heating value (kcal/kg)	4510	S	0.001
Lower heating value (kcal/kg)	4250		
Ash composition (wt%)			
SiO_2	51.08		
CaO	29.13		
Al_2O_3	11.7		
MgO_2	3.8		
TiO_2	3.1		
Na_2O	1.01		
PbO	0.25		

[a]Calculated by difference

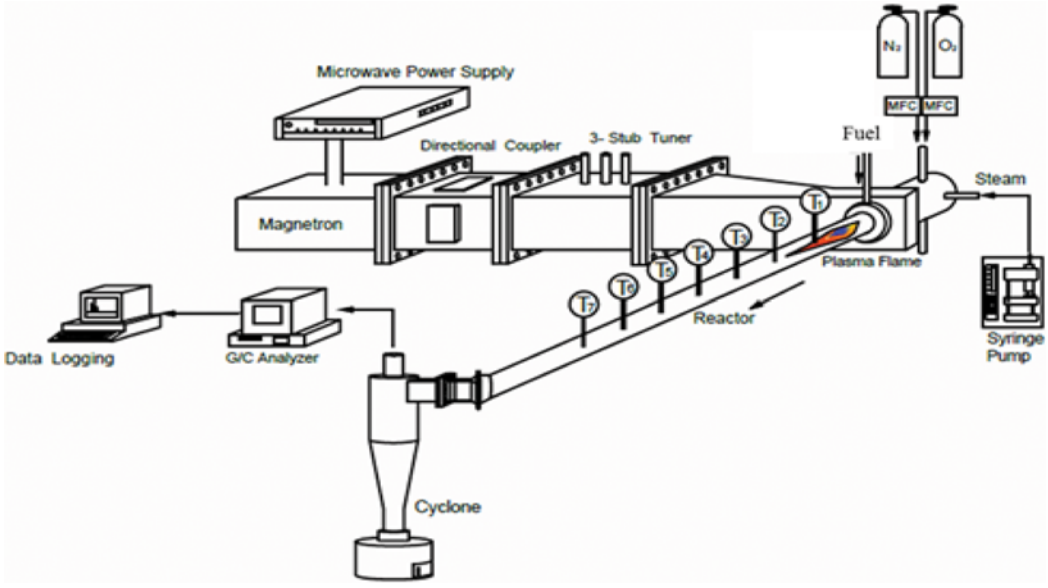

Fig. 1. Schematic diagram of 2 kW microwave plasma reactor [13].

2. Apparatus and Procedures

Gasification experiments were carried out in a microwave plasma reactor equipped with microwave generator (2.45 GHz, SM 745, Richardson Electronics) as shown in Fig. 1 [13]. The apparatus consists of a fuel feeder, microwave generator, water supply gear pump, gasifying agent feeder, gasification reactor, steam supplier, fine dust filter, and gas suction diaphragm pump. The microwave plasma gasifier (0.0254 m, id) was horizontally located on the system. Nitrogen was used as a plasma forming gas. GFRP waste particles were injected into the reactor perpendicularly, using a screw feeder. The nitrogen and GFRP mass flow rates were determined to be 16.5 L/min and 0.8 g/min, respectively. Using a mass flow controller (MFC), oxygen used as an oxidant was introduced into the plasma reactor with a range of operational flow rates of up to 1.7 L/min. The plasma power was controlled between 1 and 1.8 kW. Steam, used as a gasifying agent, was injected into the reactor using the gear pump operating between 0 and 0.8 mL/min. To maintain temperatures greater than 120 °C, the steam feed-line was covered with a band heater. The plasma forming gas, oxygen, and steam were then fed into the gasifier via a vortex that enhanced the plasma stability. The syngas from GFRP gasification reaction was passed through a fine dust filter. The gas was introduced into a gas chromatograph (GC; HP6890, Agilent) containing Carbosphere column, and was analyzed with a thermal conductivity detector (TCD).

The results of the GC analysis were collected and stored in real time, and the gaseous products were passed through a hood system. To observe microscopic interactions between the ash and polymer phases, the surface structure of the GFRP char was investigated by scanning electron microscopy (SEM; 535M, Philips).

RESULTS AND DISCUSSION

1. Effect of Oxygen/Fuel Ratios

Partial oxidation and combustion are prevalent reactions occurring within gasified fuel containing highly volatile compounds.

Fig. 2 shows how varying the oxygen/fuel ratio alters the composition of the syngas generated at a plasma power of 1.4 kW and no steam supply. With an increasing oxygen/fuel ratio, the amount

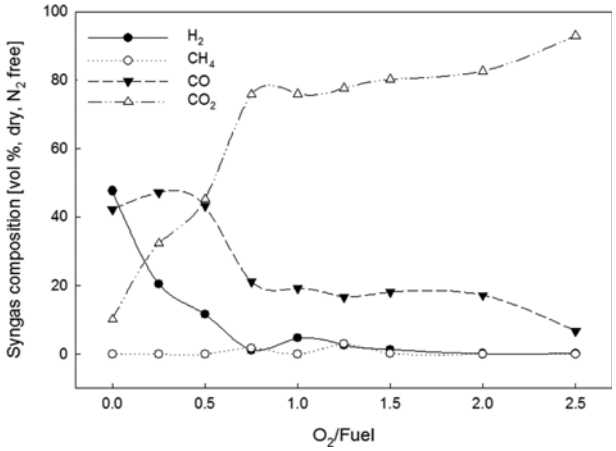

Fig. 2. Effect of oxygen supply on syngas composition at S/F: 0, Power: 1.4 kW.

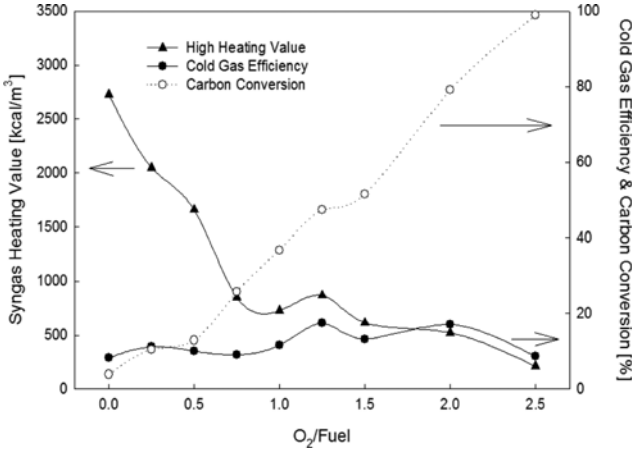

Fig. 3. Effect of oxygen supply on syngas heating value, carbon conversions, cold gas efficiency at S/F: 0, Power: 1.4 kW.

of hydrogen and carbon monoxide decreased, whereas the carbon dioxide increased. Methane consistently comprised less than 3%, regardless of the oxygen/fuel ratio.

$$C+\frac{1}{2}O_2 \rightleftharpoons CO \quad \Delta H=-110 \text{ kJ/mol} \tag{1}$$

$$C+O_2 \rightleftharpoons CO_2 \quad \Delta H=-394 \text{ kJ/mol} \tag{2}$$

Increasing the oxygen supply, the reactions denoted by Eqs. (1) and (2) were shifted to favor the production of carbon monoxide and dioxide, respectively.

Fig. 3 illustrates how varying oxygen supply affects the high heating value of the syngas, carbon conversion and cold gas efficiency of the GFRP plasma gasification. The carbon conversion (X_c) and cold gas efficiency (η), which is the thermodynamic efficiency indicator of the gasification process, are defined as follows:

$$X_c\,(\%)=\frac{\text{Mass flow of carbon in the syngas}}{\text{Mass flow of carbon in the feedstock}}\times 100 \tag{3}$$

$$\eta\,(\%)=\frac{\text{Mass flow rate of syngas}\times\text{higher heating value of syngas}}{\text{Mass flow rate of feedstock}\times\text{higher heating value of feedstock}}\times 100 \tag{4}$$

Carbon conversion increased with increasing oxygen supply and decreased with increasing heating value. Increased carbon dioxide production was directly attributed to a decline in the high heating value of syngas. It shows that the combustion reactions occurring in the presence of stoichiometric or excess oxygen contain more than 6% carbon monoxide and less than 92% carbon dioxide.

The cold gas efficiencies reported in this study are much lower than those reported for glycerol plasma gasification because the high specific heat of ash on GFRP inhibits heat transfer to the polymer [13] which was experimented in the 2 kW microwave plasma reactor. Compared with a physical bonding force for the solid fuel, the low molecular bonding force of liquid fuel favored thermal reaction such as a partial oxidation in high temperature. Therefore, the solid fuel gasification reaction was less dominated than a liquid fuel reaction. A strong vortex was presented in the region where fuel

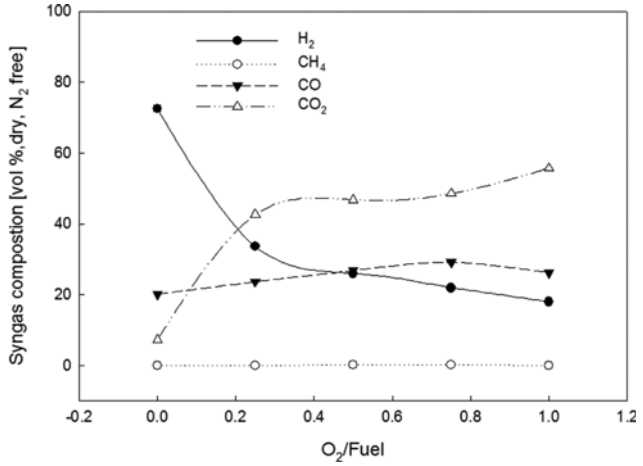

Fig. 4. Effect of oxygen supply on syngas composition at S/F: 1, Power: 1.4 kW.

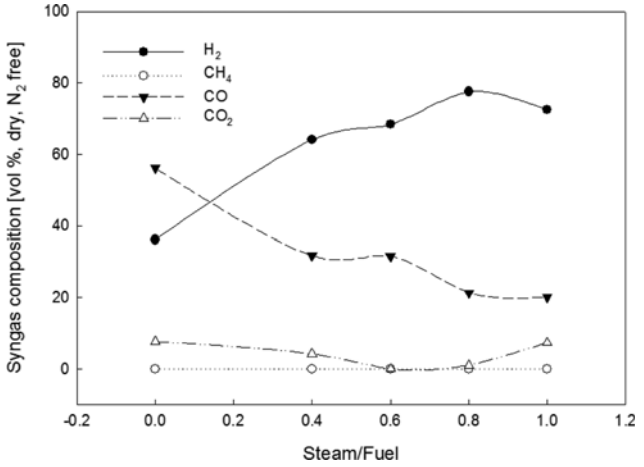

Fig. 6. Effect of steam on syngas composition at O_2/F: 0, Power: 1.4 kW.

particles were introduced into the plasma gasifier. The strong centrifugal force prevented fuel particles from flowing into plasma flame core, wherein the temperature is the highest.

Fig. 4 depicts the composition of the syngas at a plasma power of 1.4 kW and a steam/fuel ratio of 1 changes with the oxygen/fuel ratio. With increasing oxygen supply, the carbon monoxide content decreased from 26% to 20%, whereas the carbon dioxide content increased from 7% to 52%. Although the steam reforming reaction increased with oxygen supply, high oxygen levels also promoted oxidation reactions. The carbon monoxide content increased up to 29% with oxygen/fuel ratios between 0.2 and 1 due to partical combustion (Eq. (1)) and strong Boudouard reaction [14] as follows.

$$C + CO_2 \rightleftharpoons 2CO \quad \Delta H = +172.5 \text{ kJ/mol} \tag{5}$$

The effects of varying the oxygen/fuel ratio at a power of 1.4 kW and a steam/fuel ratio of 1 on the syngas high heating values, cold gas efficiencies, and carbon conversions are shown in Fig. 5. With increasing the oxygen supply, cold gas efficiencies increased up to an oxygen/fuel ratio of 0.5, beyond which these efficiencies decreased. The syngas high heating values ranged from 1,300 to 2,800 kcal/Nm^3. Increasing the oxygen/fuel ratio from 0 to 0.2 gave rise

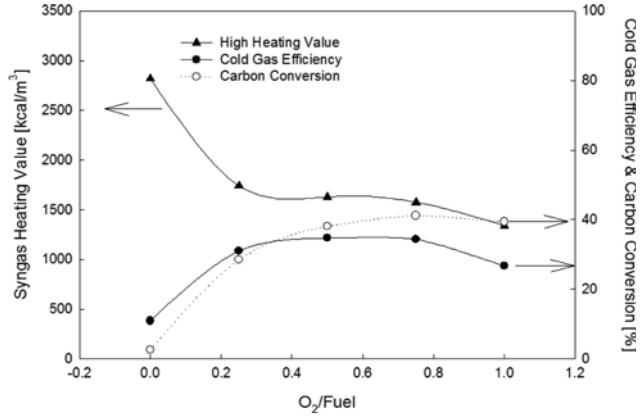

Fig. 5. Effect of oxygen supply on syngas heating value, carbon conversions, cold gas efficiency at S/F: 1, Power: 1.4 kW.

to partial oxidation and combustion reactions. Throughout this range, syngas heating values declined due to both the decreased production of hydrogen and increased production of carbon dioxide.

2. Effect of Steam/Fuel Ratios

The effect of the steam/fuel ratio on syngas composition at a plasma power of 1.4 kW and no oxygen supply is shown in Fig. 6.

With increasing steam supply, hydrogen production increased while carbon monoxide production gradually decreased.

$$C + H_2O \rightleftharpoons H_2 + CO \quad \Delta H = +131 \text{ kJ/mol} \tag{6}$$

$$CO + H_2O \rightleftharpoons H_2 + CO_2 \quad \Delta H = -42 \text{ kJ/mol} \tag{7}$$

The reactions represented by Eqs. (6) and (7) occur within the conventional gasifier [14,15]. The endothermic reaction, Eq. (6), is thought to occur upstream at high temperature, while the exothermic reactions Eqs. (1) and (7) are likely to occur downstream at low temperature.

Reactions, involving electrons, radicals, and ions, promoted by the plasma flame, are described by Eqs. (8) and (9).

$$H_2O + e \longrightarrow OH\cdot + H\cdot + e \tag{8}$$

$$C_xH_y + H\cdot \longrightarrow C_xH_{(y-1)}\cdot + H_2 \tag{9}$$

Within the steam, water molecules bombarded by electrons dissociate into hydroxyl (OH·) and hydrogen (H·) radicals. The H· radicals then react with hydrocarbons to generate hydrocarbon radicals and H_2 [16]. Increasing the flow rate of the steam favors the reaction represented by Eq. (8), resulting in increased production of H_2. Free electrons are therefore essential to sustain the steam reforming reaction. A steam supply increase maintained the gradual temperature gradient although the highest temperature in the reactor was decreased for the reactions represented by Eqs. (6) and (7).

Fig. 7 shows how varying the steam supply affects the GFRP syngas high heating value, cold gas efficiency, and carbon conversion. The high heating value was largely unaffected by the steam supply, ranging from 2,700 to 3,100 kcal/Nm^3. The graph shows that the cold gas efficiencies changed from 5% to 12% and the carbon conversion ranged from 1% to 7%.

The composition and concentration of the syngas evolved from

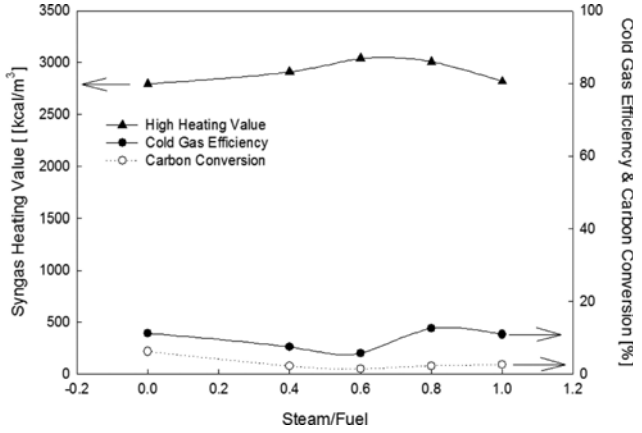

Fig. 7. Effect of steam on syngas heating value, carbon conversions, cold gas efficiency at O_2/F: 0, Power: 1.4 kW.

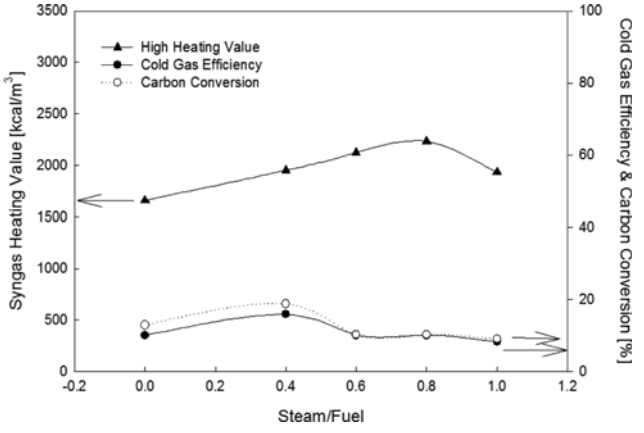

Fig. 9. Effect of steam supply on syngas heating value, carbon conversions, cold gas efficiency at O_2/F: 0.5, Power: 1.4 kW.

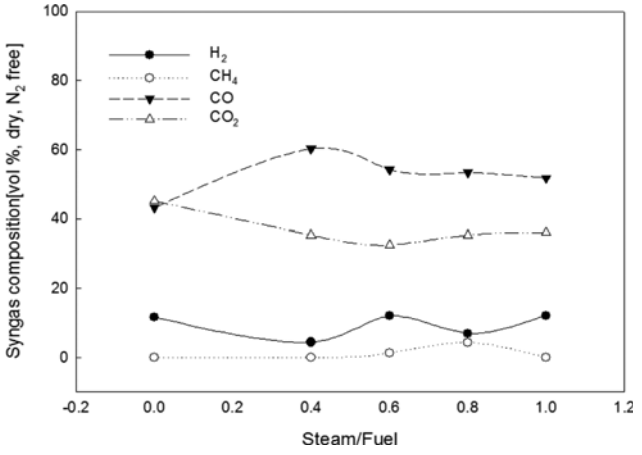

Fig. 8. Effect of steam supply on syngas composition at O_2/F: 0.5, Power: 1.4 kW.

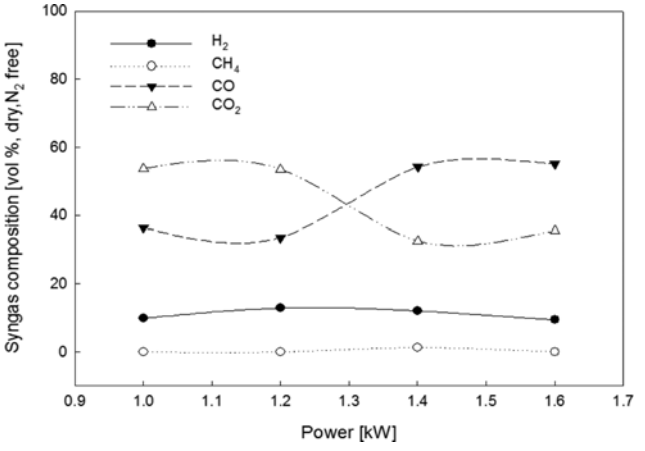

Fig. 10. Effect of plasma power on syngas composition at O_2/F: 0.5, S/F: 0.6.

the GFRP plasma gasifier are described in Fig. 8 as an effect of the steam/fuel ratio at power 1.4 kW and an oxygen/fuel ratio of 0.5. The data shows that the gas contained 4-11% hydrogen, 43-60% carbon monoxide, and 32-45% carbon dioxide.

Although carbon monoxide and hydrogen were generated by the water-gas shift reaction, combustion also contributed to a decreasing syngas heating value. More energy was spent in forming both steam and nitrogen plasma than in forming pure nitrogen plasma [17]. While an increased supply of steam produced unsustainable plasma, the steam region expanded to downstream on the plasma gasifier because of the longer flame length, which resulted in partial oxidation and combustion.

$$C_mH_n + aH_2O \longrightarrow bH_2 + cCO + dC_{m1}H_{n1} \quad (10)$$

$$C_{m1}H_{n1} + eH_2O \longrightarrow fH_2 + gCO \quad (11)$$

As the steam reforming reaction proceeded at temperatures in excess of 900 °C, the strong polymer matrix changed to a low molecular weight compound in GFRP [18]. Both hydrogen and carbon monoxide were produced by these reactions.

Fig. 9 shows that the cold gas efficiencies and carbon conversions were less than 20%. Steam reforming reactions evidently influenced the heating values. Although high heating values increased with steam supply in the conventional gasifier, the heating value was not altered dramatically [19].

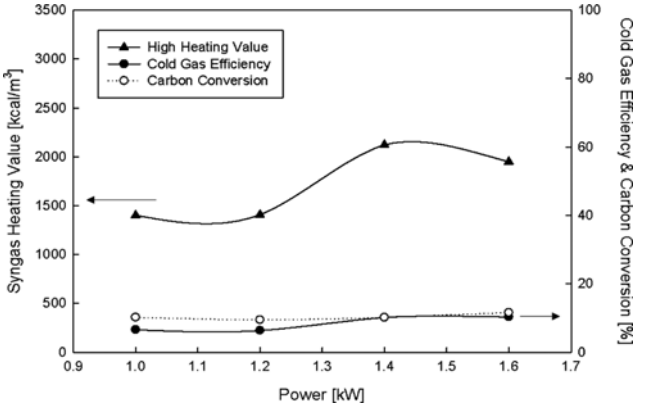

Fig. 11. Effect of plasma power on syngas heating value, carbon conversions, cold gas efficiency at O_2/F: 0.5, S/F: 0.6.

3. Effect of Plasma Power

Plasma power was one of the experimentally determined parameters that critically affected the gasification performance. Power correlated well with reactor temperature size of the plasma, and electron density [9]. In particular, an increase in the concentration of reactive particles, such as electrons, radicals, and ions affected the composition of the syngas and the thermodynamic efficiency.

Fig. 10 shows how the product gas within the reactor varies with power using at a steam/fuel ratio of 0.6 and an oxygen/fuel ratio of 0.5. Hydrogen and methane concentrations did not vary much with changes in plasma power. Increasing the power from 1.2 to 1.4 kW resulted in increased production of carbon monoxide from 33 to 46%, whereas carbon dioxide production was reduced from 53 to 32%.

Increasing the plasma power also contributed to a decline in the production of carbon dioxide, an incombustible greenhouse gas, con-

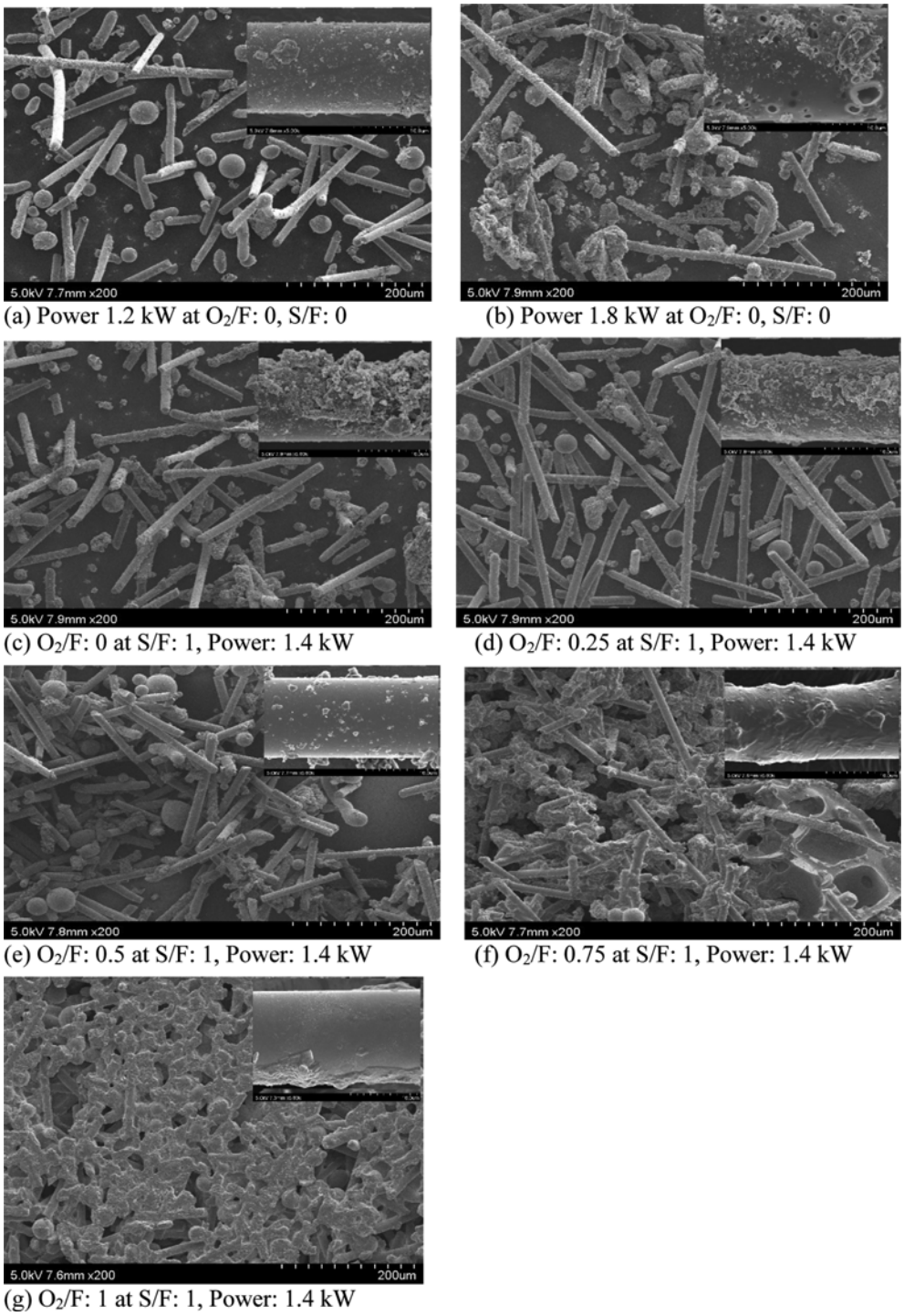

Fig. 12. SEM image of GFRP char obtained by a pyrolysis, partial oxidation, and combustion.

current with increased electron density and gas temperature within the reactor [20], wherein the following reaction occurs [21,22]:

$$CO_2 + e \longrightarrow CO_2^* + e \longrightarrow CO + O + e, \ ^*: \text{excited condition.} \quad (12)$$

The increased power was proven to be critical to activating the radical and ion reactions since this prevented the enlarged plasma flame from losing too much heat to the dominant endothermic reactions denoted by Eqs. (1), (5) and (6).

Fig. 11 illustrates the effect of plasma power on carbon conversion, heating value, and cold gas efficiency from the GFRP gasifier at an oxygen/fuel ratio of 0.5 and steam/fuel ratio of 0.6. Increasing the power from 1.2 to 1.4 kW increased the high heating value from 1,400 to 2,100 kcal/Nm^3, while the cold gas efficiency increased from 6 to 10% and the carbon conversion ranged from 9 to 11%. The increasing production of carbon monoxide contributed to a higher heating value and cold gas efficiency. In spite of a plasma power increase, the relatively constant cold gas efficiency implies that plasma power was not the most important variable affecting GFRP heat-chemical reactions.

4. Char Surface Characteristics

The SEM images of the char products of GFRP pyrolysis between 1.2 and 1.8 kW are shown in Figs. 12.

The images illustrate that the polymer-coated cylindrical pillar is composed mainly of SiO_2- and Al_2O_3-rich ash. With increasing plasma power, the GFRP chars were found to swell, as is evident from these pictures. The sharp temperature gradient between the plasma flame and the GFRP simulates heat diffusion and devolatilization. Bubble marks and the swelled structure, which had porous shape such as biomass and coal char, were observed in the char produced using 1.8 kW of power [23-25].

The images of the char produced by varying the oxygen/fuel ratio from 0 to 1 at power of 1.4 kW and a steam/fuel ratio of 1 are presented in Figs. 12(c) to 12(g). With increasing oxygen supply, the polymer gradually underwent oxidative decomposition. Beyond stoichiometric combustion, the polymer remained largely attached to a pillar. Lopez and Kelly reported that a polymer attached to a pillar was largely decomposed at a relatively low reactor temperature [26,27]. We explained that the residence time was more important variable in GFRP polymer decomposition than a reactor temperature.

The rapid heating of fuel on the surface altered the polymer structure, effecting its cross-linking at high-temperature, thereby enhancing the degree of adhesion between the ash and polymer matrix. Such increased thermochemical bonding between the ash and polymer phases inhibited further decomposition of the polymer matrix.

CONCLUSION

The effects of plasma power (1-1.8 kW), oxygen/fuel (0-2.5) and steam/fuel ratios (0-1) on the gasification characteristics of GFRP wastes in a microwave plasma reactor have been determined. While the carbon conversion increased with increasing oxygen supply, the syngas heating value and cold gas efficiency decreased due to combustion. Increasing the steam supply produced more hydrogen by facilitating the water-gas shift and ion reforming reactions. Increasing the plasma power resulted in the conversion of carbon dioxide to carbon monoxide. After increasing the oxygen/fuel ratio, the polymer molecules attached to the pillar were decomposed, and increasing oxidation reduced the polymer in GFRP.

ACKNOWLEDGEMENT

This work was conducted under the framework of Research and Development Program of the Korea Institute of Energy Research (KIER) (B4-2481-07). This work was also supported by the New & Renewable Energy Core Technology Program of the Korea Institute of Energy Technology Evaluation and Planning (KETEP) granted financial resource from the Ministry of Trade, Industry & Energy, Republic of Korea (No. 20143030090960). Also, this work was also supported by the National Research Council of Science & Technology (NST) grant by the Korea government (MSIP) (No. CRC-15-07-KIER).

REFERENCES

1. B. Jahn and E. Witten, The global CRP 2013 Report (Market development, trends challenges and opportunities), Sept (2013).
2. L. Gray, MANE-6960- Solid and Hazardous waste prevention and control Engineering, Renselaer Hartford, U.S.A. (2014).
3. S. H. Jung, M. H. Cho, B. S. Kang and J. S. Kim, *Fuel. Process. Technol.*, **91**, 277 (2010).
4. J. S. Bae, D. W. Lee, S. J. Park, Y. J. Lee, J. C. Hong, C. Han and Y. C. Choi, *Korean J. Chem. Eng.*, **30**(2), 321 (2013).
5. A. Noma, M. Mawatati, C. Goto, Y. Hoshi, K. Inoue and K. Yoshikawa, *Ind. Eng. Chem.*, **45**, 5127 (2006).
6. Y. Kuo, C. T. Wang, C. H. Tsai and L. C. Wang, *J. Hazard. Mater.*, **162**, 469 (2009).
7. H. S. Uhm, Y. C. Hong and D. H. Shin, *Plasma Sources Sci. Technol.*, **15**(2), S26 (2006).
8. J. R. Roth, Industrial Plasma Engineering, London: Institute of Physics (1945).
9. Y. C. Hong, S. J. Lee, Y. J. Kim, B. J. Lee, S. Y. Cho and H. S. Chang, *Energy,* **47**, 36 (2012).
10. S. J. Yoon and J. G. Lee, *Int. J. Hydrogen. Energy*, **37**, I7093 (2012).
11. J. L. Shie, L. X. Chen, K. L. Lin and C. Y. Chang, *Energy,* **66**, 82 (2014).
12. L. Tang and H. Huang, *Fuel*, **84**, 2055 (2005).
13. S. J. Yoon, Y. M. Yun, M. W. Seo, Y. K. Kim, H. W. Ra and J. G. Lee, *Int. J. Hydrogen. Energy,* **38**, I4559 (2013).
14. P. Basu, Combustion and gasification in fluidized beds, Boca Raton: Taylor and Francis (2006).
15. J. Huang and D. Ibrahim, *Int. J. Hydrogen. Energy*, **39**, 3294 (2014).
16. D. Levko, A. Shchedrin, V. Chernyak, S. Olszewski and O. Nedybaliuk, *J. Phys. D: Appl. Phys.*, **44**, 145206 (2011).
17. M. Hrabovsky, *The Open Plasma Physics J.*, **2**, 99 (2009).
18. Q. Zhang, L. Dor, D. Fenigshtein, W. Yang and W. Blasiak, *Appl. Energy* (2011), DOI:10.1016/j.penergy.2011.01.041.
19. R. Govind and J. Shah, *AIChE J.*, **30**(1), 79 (1984).
20. S. Moon and W. Choe, *Phys. Plasma*, **9**, 4045 (2002).
21. L. Spencer and A. Gallimore, *Plasma Chem. Plasma Process* (2010), DOI:10.1007/s1 1090-010-9273-0.
22. C. Liu and G. Xu, *Fuel. Process. Technol.*, **58**, 119 (1999).

23. R. K. Sharma, J. B. Wooten, V. L. Baliga and M. R. Hajaligol, *Fuel*, **80**, 1825 (2001).
24. M. A. Sukiran, L. S. Kheang, N. A. Bakar and C. Y. May, *Am. J. Appl. Sci.*, **8**(10), 984 (2011).
25. J. Bae, D. Lee, Y. Lee, S. Park, J. Park, J. Hong, J. Kim, P. Yoon, H. Kim, C. Han and Y. Choi, *Powder Technol.*, **254**, 72 (2014).
26. R. M. Kelly, J. R. Kennerley and C. D. Rudd, *Compos. Sci. Technol.*, **60**, 509 (2000).
27. F. A. Lopez, M. I. Martin, F. J. Alguacil, J. M. Rincon, T. A. Centeno and M. Romero, *J. Anal. Appl. Pyrol.*, **93**, 104 (2012).